

---

# Dynamical Anatomy of NARMA10 Benchmark Task

---

**Tomoyuki Kubota**  
The University of Tokyo  
t.kubota@ne.t.u-tokyo.ac.jp

**Kohei Nakajima**  
The University of Tokyo

**Hirokazu Takahashi**  
The University of Tokyo

## Abstract

The emulation task of a nonlinear autoregressive moving average model, i.e., the NARMA10 task, has been widely used as a benchmark task for recurrent neural networks, especially in reservoir computing. However, the type and quantity of computational capabilities required to emulate the NARMA10 model remain unclear, and, to date, the NARMA10 task has been utilized blindly. Therefore, in this study, we have investigated the properties of the NARMA10 model from a dynamical system perspective. We revealed its bifurcation structure and basin of attraction, as well as the system's Lyapunov spectra. Furthermore, we have analyzed the computational capabilities required to emulate the NARMA10 model by decomposing it into multiple combinations of orthogonal nonlinear polynomials using Legendre polynomials, and we directly evaluated its information processing capacity together with its dependences on some system parameters. The result demonstrates that the NARMA10 model contains an unstable region in the phase space that makes the system diverge according to the selection of the input range and initial conditions. Furthermore, the information processing capacity of the model varies according to the input range. These properties prevent safe application of this model and fair comparisons among experiments, which are unfavorable for a benchmark task. As a result, we propose a benchmark model that can clearly evaluate equivalent computational capacity using NARMA10. Compared to the original NARMA10 model, the proposed model is highly stable and robust against the input range settings.

## 1 Introduction

Nonlinear autoregressive moving average (NARMA) tasks have been introduced to test the performance of recurrent neural networks (RNN)[1]. These tasks evaluate how well the RNN can emulate the NARMA model. The NARMA10 task has been widely used as a benchmark task for reservoir computing (RC) [2–17]. RC[16, 18, 19] is a framework for RNN training, where nodes are often described by sigmoid neurons, recurrently connect each other with randomized weights, and form a network (referred to as a reservoir). Inputs to nodes are time-series signals that multiple the original input signals by weights specific to each node. The nodes update their states using the inputs and their previous states, and they asymptotically converge a trajectory without dependence on the initial values, and the outputs are calculated by linearly combining the states with a readout weight vector. RC trains the readout weight to emulate the desired outputs. The NARMA10 task was developed to compare the performance of various RNNs and has been used in many situations. For example, the performance of echo state networks (ESN) has been tested using the NARMA10 task [10, 15, 16]. This task is also used to evaluate the computational capability of physical systems, e.g., laser systems[2], opto-electronic architectures[14], carbon nanotubes[20], soft robotic

systems[11, 12], and more[4, 6, 8, 13, 17]. Thus, the NARMA10 task is one of the most representative benchmark tasks and can be used effectively to evaluate the computational capabilities of dynamical system. However, the type and quantity of computational capabilities required to emulate the desired output are unknown.

The computational capabilities of a dynamical system are decomposed into properties to store input streams and to nonlinearly process them[21]. To emulate the desired outputs, the reservoir must have enough memory of historical inputs and transform them nonlinearly. These features are evaluated by using information processing capacity, which represents how precisely and how long the reservoir retains historical inputs. Here, the input is composed of terms in input stream’s Legendre polynomial, whose combination represents nonlinear transformation.

Furthermore, the NARMA10 task includes input intensity and range parameters, which change the output and should alter the computational capabilities. However, researchers frequently use individual settings, which may cause one to evaluate different computational capabilities. For example, the input range is a controllable parameter, where a uniform random number is often used for input  $u_k$ , and two main ranges are adopted, i.e.,  $[0.0, 0.5]$  [1, 2, 4, 5, 7–10, 14, 15] and  $[0.0, 1.0]$  [3, 11, 13, 16, 17]. Both two settings were utilized when ESNs emulated the NARMA10 model in [10, 16]. As a result, their normalized root mean square errors differ, which indicates that parameter settings may affect their computational capabilities.

This study has two objectives: 1) analyze the properties of the NARMA10 model as a dynamical system to examine the specification of parameters for a benchmark task, and 2) clarify the type and quantity of computational capabilities required to emulate the NARMA10 model.

In Sec. 2, we provided methods to investigate properties of the NARMA10 model as a dynamical system by analyzing Lyapunov spectra, bifurcation structure, basin of attraction, and stability regions. We then explained how to estimate the information processing capacity. In Sec. 3, we revealed the properties of NARMA10 and the capacity with the methods, and thus we found NARMA10’s problems as a benchmark task. In addition, we introduced a novel model to resolve the problems with the NARMA10 model.

Table 1: Derivative table of  $\Delta w_1$  and  $\Delta w_2$  in stability diagram (Figure S1(g))

# area	$\Delta w_1$	$\Delta w_2$	# area	$\Delta w_1$	$\Delta w_2$	# area	$\Delta w_1$	$\Delta w_2$
(i)	-	-	(iii)	-	+	(v)	-	+
(ii)	+	-	(iv)	+	+	(vi)	-	-

## 2 Methods

### 2.1 NARMA10 benchmark task

The NARMA10 emulation task is a benchmark task for reservoir computing. Here, the desired output is given as follows:

$$y_{k+1} = \alpha y_k + \beta y_k \sum_{i=0}^9 y_{k-i} + \gamma u_k u_{k-9} + \delta, \quad (1)$$

$$u_k = \mu + \sigma \nu_k, \quad (2)$$

where the default constant parameters  $(\alpha, \beta, \gamma, \delta)$  are set to  $(0.3, 0.05, 1.5, 0.1)$ , and  $\nu_k, \mu$ , and  $\sigma$  are the input at the  $k$ -th time step, the average of  $\nu_k$ , and the input intensity parameter, respectively. Note that  $\nu_k$  follows uniform distribution in the range  $[-1, 1]$ . Here, all initial values  $y_k$  ( $k = 0, \dots, 9$ ) were set to zero except when the basin of attraction was examined.

### 2.2 Lyapunov spectrum

The sensitivity to initial values is evaluated by the Lyapunov spectrum, which exhibits how exponentially two distances beginning from close points grow or shrink. To consider the stability of NARMA10 dynamics, the Lyapunov spectra were computed. We defined new variables for a time-delay system as  $z_{i,k} \equiv y_{k+1-i}, i = 1, \dots, 10$  and summarized them as vector  $\mathbf{z}_k = [z_{1,k} \dots z_{10,k}]^T$ .

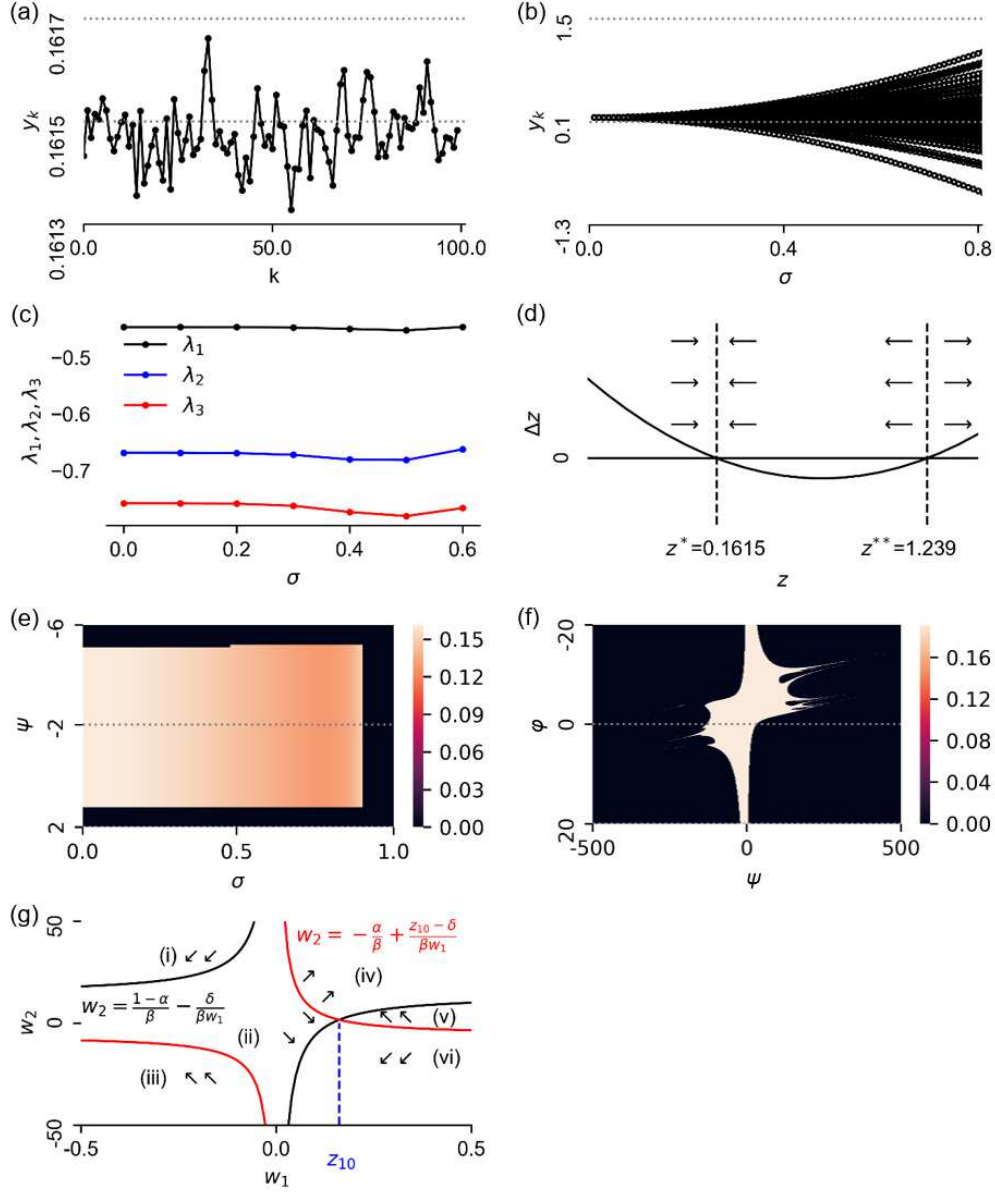


Figure 1: Properties of NARMA10 dynamical system with  $(\alpha, \beta, \gamma, \delta) = (0.3, 0.05, 1.5, 0.1)$ . (a) Time-series of Eq.(6) in  $\sigma = 0.01$ . (b) Bifurcation diagram of Eq.(6). (c) Three largest Lyapunov spectra  $\lambda_i, i = 1, 2, 3$  relative to  $\sigma$  are shown. (d) Stability diagram of  $z$  in vicinity of equilibria.  $\Delta z = (\alpha - 1)z + 10\beta z^2 + \delta$ . (e) Basin of attraction of Eq.(6) relative to  $\sigma$  and  $\psi$ . In (e) and (f), each dot shows  $y_k$  at  $k = 5999$  on a heat map, where the black area represent divergence to infinity. The initial values were  $y_i = \psi, i = 0, \dots, 9$ , and  $\sigma$  was 0.2. (f) Basin of attraction of Eq.(6) relative to  $\psi$  and  $\phi$ . The initial values were set to  $y_0 = \psi$  and  $y_i = \phi, i = 1, \dots, 9$ . (g) Stability diagram of  $w_1 = z_1$  and  $w_2 = \sum_{i=1}^{10} z_i$  as  $z_{10} > \delta$ . The signs of  $\Delta w_1$  and  $\Delta w_2$  are shown in Table S1. Note that point  $(z_{10}, (1 - \alpha)/\beta - \delta/\beta z_{10})$  is a saddle point.

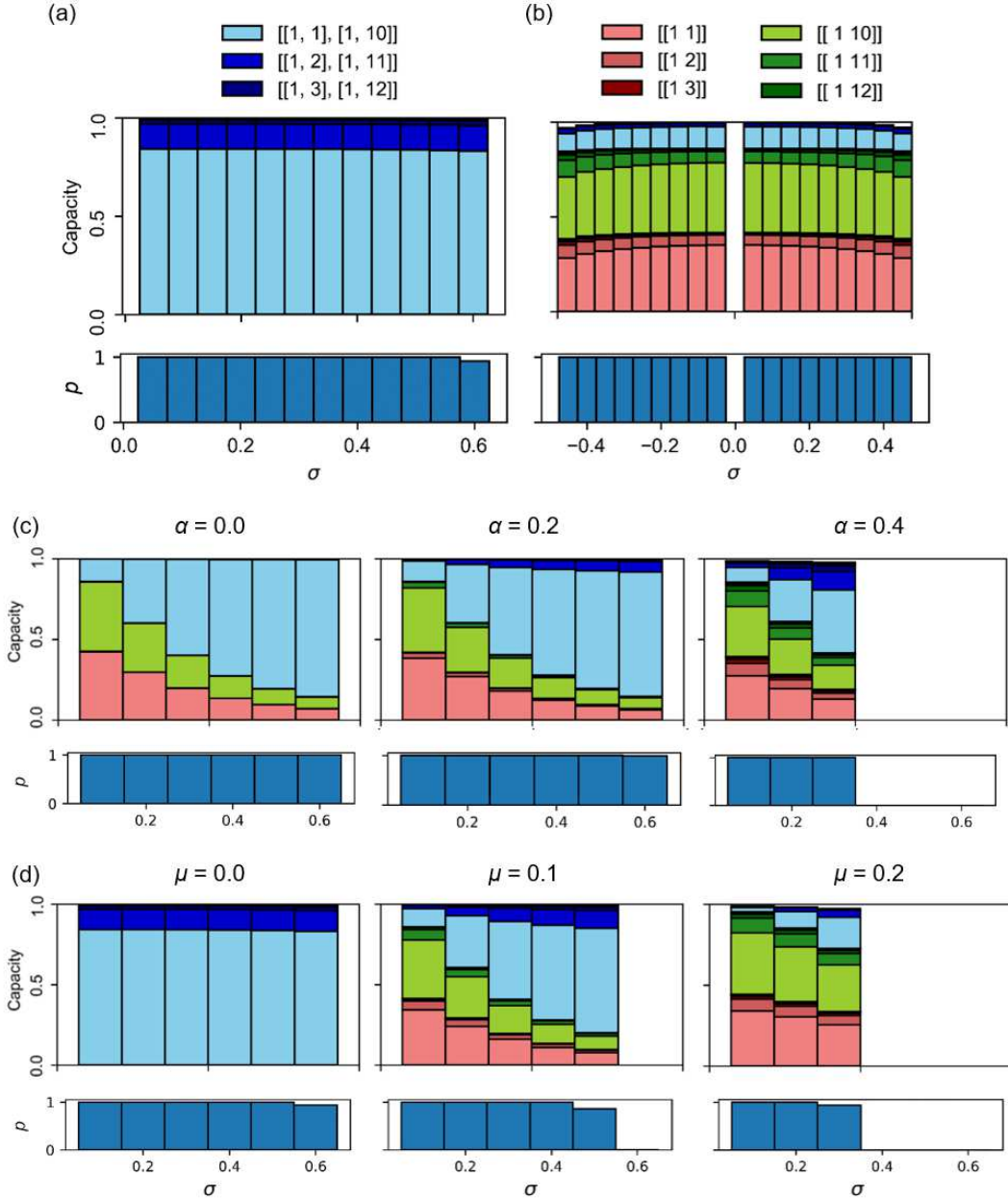


Figure 2: IPC distribution relative to  $\sigma$ , and  $p$  probability that  $y_k$  does not diverge. The labels indicate representative combinations of  $[[n_i, k_i]]$ , where  $n_i$  is the degree of polynomial,  $k_i$  is the delayed time step of input, and the desired output is  $\prod_i \mathcal{P}_{n_i}(\nu_{k_i})$ , and labels for other combinations are omitted. The probability  $p$  represents the proportion of  $y_k$  not diverging to infinity using 100 input time-series  $\nu_k$  which were generated from 100 random seeds. In all figures, capacities are not stacked if the output diverged or  $\sigma = 0$ . In (a) and (b), the two ranges of  $u_k$  are as follows: (a)  $(\alpha, \beta, \gamma, \delta, \mu) = (0.3, 0.05, 1.5, 0.1, 0.0)$ , i.e.,  $(\alpha, \beta, \gamma, \delta)$  are default and  $u_k$  follows uniform distribution in the range  $[-\sigma, \sigma]$ . (b)  $(\alpha, \beta, \gamma, \delta, \mu) = (0.3, 0.05, 0.375, 0.1, \sigma)$ , which is equivalent to the condition that  $(\alpha, \beta, \gamma, \delta)$  are default and  $u_k$  follows uniform distribution in the range  $[0, \sigma]$  ( $\sigma > 0$ ) or  $[\sigma, 0]$  ( $\sigma < 0$ ). (c), (d), and (e) show the capacity relative to  $\alpha$ ,  $\beta$ , and  $\mu$ , respectively, and fixed parameters  $(\alpha, \beta, \gamma, \delta, \mu)$  were set to  $(0.3, 0.05, 1.5, 0.1, 0.1)$ .

Here, Eq. (6) was rewritten as Eq. (3) and (4) as follows:

$$z_{1,k+1} = \alpha z_{1,k} + \beta z_{1,k} \sum_{i=1}^{10} z_{i,k} + \delta. \quad (3)$$

$$z_{j,k+1} = z_{j-1,k} \quad (j = 2, \dots, 10). \quad (4)$$

The Jacobian of Eq. (6)  $\mathbf{J}_k$  is described with  $\mathbf{z}_k$  as follows:

$$\mathbf{J}_k = \frac{\partial \mathbf{z}_{k+1}}{\partial \mathbf{z}_k} = \begin{bmatrix} \mathbf{W}_k & \mathbf{Y}_k \\ \mathbf{I}_9 & \mathbf{O}_{9 \times 1} \end{bmatrix}, \quad (5)$$

where  $\mathbf{W}_k = [X_k \ Y_k \ \dots \ Y_k] \in \mathbb{R}^9$ ,  $X_k = \alpha + 2\beta z_{1,k} + \beta \sum_{i=2}^{10} z_{i,k}$ ,  $Y_k = \beta z_{1,k}$ .  $\mathbf{I}_9$  and  $\mathbf{O}_{9 \times 1}$  represent  $9 \times 9$  identity matrix and  $9 \times 1$  zero matrix, respectively. With the Jacobian matrices, the Lyapunov spectrum was computed as follows:

$$\lambda_i = \frac{1}{T} \sum_{k=1}^T \ln \rho_i(\mathbf{J}_M \mathbf{J}_{M-1} \cdots \mathbf{J}_1) \quad (i = 1, \dots, 10), \quad (6)$$

where  $\rho_i(\mathbf{J}_M \mathbf{J}_{M-1} \cdots \mathbf{J}_1)$  is the  $i$ -th singular value of matrix  $\mathbf{J}_M \mathbf{J}_{M-1} \cdots \mathbf{J}_1$ , and  $T$  and  $M$  were set to 6000 and 40, respectively.

### 2.3 Stability analysis

When the equilibrium point of  $z_{i,k}$  ( $i = 1, \dots, 10$ ) is represented by  $z^*$ , by replacing  $z_{i,k+1}$  and  $z_{i,k}$  ( $i = 1, \dots, 10$ ) in Eq. (3) to  $z^*$ , two equilibria  $z^* = (1 - \alpha)/20\beta \pm \sqrt{\{(1 - \alpha)/20\beta\}^2 - \delta/10\beta} = 0.1615, 1.239$  are obtained. Additionally, when  $z_k = z_{1,k} = \dots = z_{10,k}$  in vicinity of  $z^*$  is assumed, according to Eq.(3),  $\Delta z_k = z_{k+1} - z_k$  is represented as follows:

$$\Delta z_k = (\alpha - 1)z_k + 10\beta z_k^2 + \delta. \quad (7)$$

Eq.(3) is represented by  $z_{1,k}$  and  $\sum_{i=1}^{10} z_{i,k}$ ; thus, we defined  $w_{1,k} = z_{1,k}$  and  $w_{2,k} = \sum_{i=1}^{10} z_{i,k}$ , and discrete derivatives  $\Delta w_{1,k} (= w_{1,k+1} - w_{1,k})$  and  $\Delta w_{2,k} (= w_{2,k+1} - w_{2,k})$  are derived from Eqs. (3) and (4) as follows:

$$\Delta w_{1,k} = (\alpha - 1)w_{1,k} + \beta w_{1,k} w_{2,k} + \delta. \quad (8)$$

$$\Delta w_{2,k} = \alpha w_{1,k} + \beta w_{1,k} w_{2,k} + \delta - z_{10,k}. \quad (9)$$

Note that the intersection point of the nullclines in Eqs.(17) and (18) is  $(w_1, w_2) = (z_{10}, (1 - \alpha)/\beta - \delta/\beta z_{10})$ .

### 2.4 Information processing capacity

To evaluate the NARMA10 model's computational capabilities, we estimated the information processing capacity (IPC)[21], which quantifies the inputs constructing a dynamical system by giving a temporally uncorrelated time-series input  $\tilde{u}_k$  to the system and emulating the products of the historical inputs. As the system is represented by one-dimensional state, the capacity  $C_T(\tilde{u}, y)$  is reduced as follows:

$$\begin{aligned} C_T(\tilde{u}, y) &= 1 - \frac{\min_w \sum_k (\tilde{u}_k - w y_k)^2}{\langle y^2 \rangle_T} \\ &= \frac{\langle \tilde{u} y \rangle_T^2}{\langle \tilde{u}^2 \rangle_T \langle y^2 \rangle_T}, \end{aligned} \quad (10)$$

where  $\langle v \rangle_T = \sum_{k=1}^T v_k / T$ , and  $y_k$  is centered by subtracting temporal average  $\langle y \rangle_T$  prior to calculating Eq.(10). All capacities for which  $C_T(\tilde{u}, y) < \epsilon$  were set to zero using truncated capacities  $C_T^\epsilon(\tilde{u}, y) = \theta(C_T(\tilde{u}, y)) C_T(\tilde{u}, y)$ , where  $\theta(\cdot)$  is the Heaviside step function. When the model runs for a long period, e.g.,  $6 \times 10^6$  time steps, most capacities are very small, e.g.  $10^{-6}$ , and some are

significantly larger. The threshold for the Heaviside function was determined as  $3.0 \times 10^{-4}$ . The input  $\tilde{u}$  is represented by the product of  $\mathcal{P}_n(\nu)$ , the normalized Legendre polynomial of degree  $n$ .

$$\tilde{u} = \prod_{\{(n_i, k_i) \mid i=1, \dots\}} \mathcal{P}_{n_i}(\nu_{k_i}) \quad (11)$$

$$\mathcal{P}_n(\nu) = \sqrt{\frac{2n+1}{2}} \frac{(-1)^n}{2^n n!} \frac{d^n}{d\nu^n} (1-\nu^2)^n \quad (n = 1, 2, \dots) \quad (12)$$

Eq.(6) ran for  $6 \times 10^6$  time steps to calculate capacity. To wash out the initial transient, the first one-third of the time-series data were discarded, and the remaining data were used to calculate Eq.(10).

### 3 Results and discussion

#### 3.1 Lyapunov spectrum

The sensitivity to initial conditions is an important factor for a benchmark task because it is relevant to the predictability of the system states. Here, sensitivity indicates that the future system state depends on even slight differences of the present state, which varies with the input of a random number series in each trial. To examine the sensitivity to initial conditions, we derived a 10-dimensional time-delay system and the Lyapunov spectra (Eq.(6)). Figure S1(c) shows the three largest Lyapunov spectra  $\lambda_i, i = 1, 2, 3$ , all of which are negative relative to  $\sigma$ , which indicates that the system does not demonstrate chaos. Therefore, NARMA10 does not hold the sensitivity of initial conditions and perturbation from the input time-series data does not alter its geometrical structure of attractor.

#### 3.2 Basin of attraction

The NARMA10 model has 10 initial values, and changing these values may alter the attractor to which the model converges, and the computational capabilities. To analyze the attractor structure of the model, we represented the model with  $(w_1, w_2)$ . Furthermore, on this  $w_1 - w_2$  plane, we plotted nullclines to examine the increase and decrease in  $w_1$  and  $w_2$  (Figure S1(g) and Table S1). As a result, we found that the model has a fixed point attractor at the saddle point  $(z_{10}, (1-\alpha)/\beta - \delta/\beta z_{10})$ . As shown in Figure S1(b), the model varies around the fixed point with different  $\sigma$ . To investigate the conditions by which the model converges to this fixed point, we ran the model over 6000 time steps and examined  $y_{5999}$  by altering the initial values  $y_0 = \dots = y_9 = \psi$  and input intensity  $\sigma$ . Figure S1(e) shows that  $y_k$  diverges to infinity when  $\psi$  or  $\sigma$  exceeds three thresholds: (i)  $\psi < -5.15$ , (ii)  $1.239 < \psi$ , and (iii)  $\sigma > 0.8$ . Here, the divergence due to exceeding the thresholds can be explained by the same reason, i.e.,  $y_k$  entering area (iv) in Figure S1(g). In area (iv), both  $\Delta w_1$  and  $\Delta w_2$  are positive, and, in most cases, when  $y_k$  enters area (iv), it diverges. In case of (i),  $y_k$  diverges because it enters area (iv) when it converges to a fixed point. Threshold (ii) corresponds to the boundary of the area (iv) and (vi) where the initial value  $(w_1, w_2)$  exists. Threshold (ii) can also be explained by Eq.(7), where all 10 variables of the time-delay system are approximated to the same variable.  $\Delta z_k = 0$  has two equilibrium points  $z^*$ , and  $z^* = 1.239$  is an unstable point that diverges when  $z_k > 1.239$ . In case of (iii), after converging to the fixed point, if a large positive input  $u_k$  continues,  $y_k$  enters area (iv) and diverges. If the runtime becomes longer,  $y_k$  diverges with a  $\sigma$  less than the threshold. In addition, if the initial values of  $y_k$  are  $y_1 = \psi$  and  $y_2 = \dots = y_9 = \phi$ , the basin of attraction has a unique structure (Figure S1(f)) because the trajectories change depending on the setting of the initial values and some trajectories enter area (iv). In Figure 2,  $p$  is the probability of not diverging for different time-series inputs. Even though  $p$  is high, the model potentially diverges. Furthermore, two typical ranges of input, i.e.,  $u_k \in [0, 0.5]$  and  $[0, 1]$  have been used for the NARMA10 task, but  $y_k$  diverges in both cases (Figure 2(b),  $\sigma = 0.5, 1.0$ ) because  $\sigma$  is relevant to average time until divergence and the runtime is very long, e.g.,  $6 \times 10^6$  time steps. Thus, the NARMA10 model can potentially diverge depending on the initial values, input time-series, and parameter settings; thus, it can not be used safely.

#### 3.3 Information processing capacity

The total IPC is expressed as the sum of each capacity for the given combination of inputs. Here, we calculated each capacity with delayed time step  $k (< 16)$  and degree  $n_i$  ( $\sum_i n_i < 9$ ). The total

IPC is one because the NARMA10 model is a one-dimensional system and the Lyapunov exponent is negative[21]. However, the distribution in IPC changes with some parameters. Figure 2(a) and 2(b) show that the capacity with  $u_k \in [0, \sigma]$  differs significantly from that with  $u_k \in [-\sigma, \sigma]$ . If the uniform random number  $u_k$  is in the symmetric range  $[-\sigma, \sigma]$  ( $(\alpha, \beta, \gamma, \delta)$  take the default values and  $\mu = 0$ ), the capacity distribution has only capacities with  $\sum_i n_i = 2$ . In contrast, if  $u_k$  is in the asymmetric range  $[0, \sigma]$  ( $(\alpha, \beta, \delta)$  are the default values and  $\gamma = 0.375$  and  $\mu = \sigma (\neq 0)$ ), capacities with  $\sum_i n_i = 1$  are also obtained because  $u_{k-9}u_k = (\sigma\nu_{k-9} + \mu)(\sigma\nu_k + \mu) = \sigma^2\nu_{k-9}\nu_k + \mu\sigma\nu_k + \mu\sigma\nu_{k-9} + \mu^2$ ; thus the first-order terms of  $\nu$  appear. With a large  $\sigma$  value, the sum of the capacities does not become one even though the Lyapunov exponent is negative because the high-order capacities cannot be identified with Heaviside function's threshold. As shown in Figure 2(d), as  $\mu$  increases, the threshold of  $\sigma$  where the model diverges becomes larger but the one-degree capacities increases. These results suggest that input  $u_k$  should be changed according to the dynamical system when one uses the NARMA10 task. For example, as the nodes of an ESN are represented by an odd function, i.e., a hyperbolic tangent, the ESN only has odd capacities[21]. From our results, while the ESN with  $u_k \in [0, \sigma]$  emulates the NARMA10 model, that with  $u_k \in [-\sigma, \sigma]$  does not reproduce it at all. In addition, Figure 2(c) shows that as  $\alpha$  increases, the probability that the model will diverge and the capacities with greater delayed time step  $k$  increase. These results indicate that careful parameter selection for the target dynamics is required because the distribution of IPC changes significantly with different parameters values.

### 3.4 Model for benchmark task

As discussed previously, the NARMA10 model is probabilistically unstable depending on the initial conditions and some parameters. Parameters  $(\alpha, \beta, \gamma, \delta, \mu, \sigma)$  do not change the outline of the nullclines and the unstable area (iv) exists; thus, there is no parameter region wherein the model will never diverge. Therefore, we propose an emulation task using an approximate model that has nearly the same capacity as NARMA10 and is robust against the input range with Legendre polynomials. From the above capacity analysis, we narrowed down the polynomial terms to  $\mathcal{P}_1(\nu_{k-i}), i = 1, 2, \dots$  and  $\mathcal{P}_1(\nu_{k-i})\mathcal{P}_1(\nu_{k-i-9}), i = 1, 2, \dots$ , which yielded significantly greater capacity. Furthermore, although the coefficients of the polynomials depend on time step  $k$ , we considered their steady states and derived coefficients  $(p, q_i, r_i), i = 1, \dots$  as follows:

$$y_k = p + \sum_{i \in N_1} q_i \mathcal{P}_1(\nu_{k-i}) + \sum_{i \in N_2} r_i \mathcal{P}_1(\nu_{k-i}) \mathcal{P}_1(\nu_{k-i-9}) \quad (13)$$

$$p = \frac{1-\alpha}{20\beta} - \sqrt{\left(\frac{1-\alpha}{20\beta}\right)^2 - \frac{\gamma\mu^2 + \delta}{10\beta}} \quad (14)$$

$$q_i = \begin{cases} \sqrt{2/3}\gamma\mu\sigma(\alpha + 11\beta p)^i & (i = 0, \dots, 8) \\ \sqrt{2/3}\gamma\mu\sigma(1 + (\alpha + 11\beta p)^9)(\alpha + 11\beta p)^i & (i = 9, \dots) \end{cases} \quad (15)$$

$$r_i = \begin{cases} (2/3)\gamma\sigma^2(\alpha + 11\beta p + \beta\gamma\mu^2)^i & (i = 0, 1) \\ (2/3)\gamma\sigma^2(\alpha + 11\beta p + \beta\gamma\mu^2)(\alpha + 11\beta p)^{i-1} & (i = 2, \dots) \end{cases} \quad (16)$$

where  $\nu_k$  follows uniform distribution in  $[-1, 1]$ , and  $N_1$  and  $N_2$  represent sets of delayed time step  $i$  for  $\mathcal{P}_1(\nu_{k-i})$  and  $\mathcal{P}_1(\nu_{k-i})\mathcal{P}_1(\nu_{k-i-9})$ , respectively. To demonstrate this model, we employ  $N_1 = \{0, 1, 2, 9, 10, 11\}$  and  $N_2 = \{0, 1, 2\}$ . Although the low-degree polynomials represent this approximate model, the time-series reproduces the original NARMA10 model well. Figure 3(a) and 3(b) show the case of  $u_k \in [-\sigma, \sigma]$  and  $u_k \in [0, \sigma]$ , respectively. In addition, increased  $\sigma$  does not make the model unstable, and the sum of the capacity keeps one even if the magnitude of  $\sigma$  is large.

However, now that the capacity distribution of NARMA10 has been clarified, it is no longer necessary to stick to NARMA10 for benchmark task, and one can examine individual IPCs of your target system.

## 4 Conclusion

We have investigated the properties of the NARMA10 model as a dynamical system by analyzing Lyapunov spectra, the bifurcation structure, basin of attraction, and stability regions. Subsequently, we examined IPC of NARMA10 model and demonstrated the relationship between capacity and the

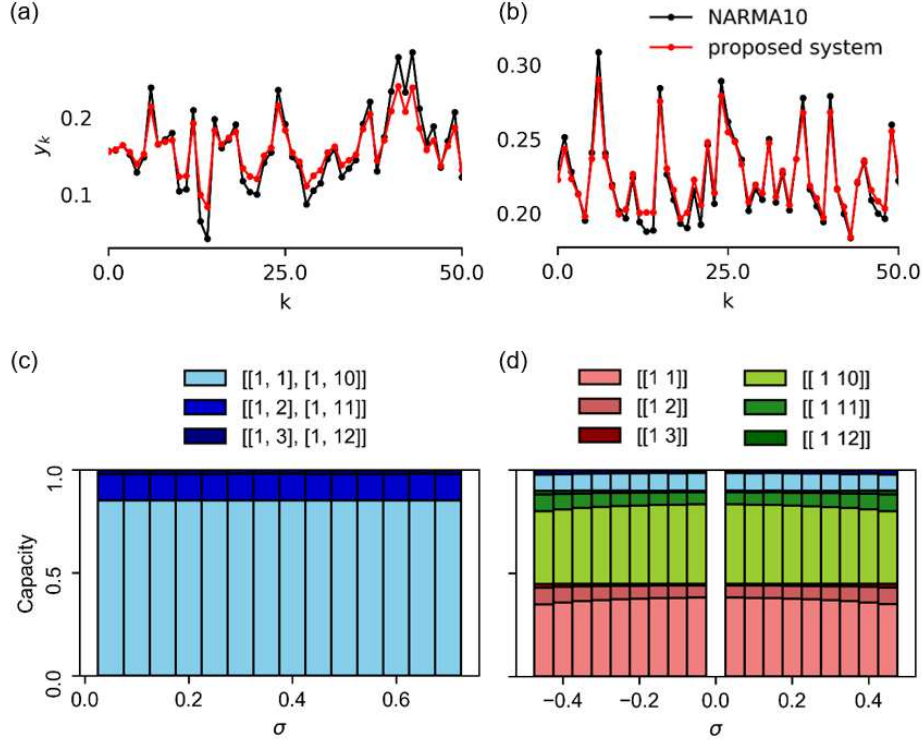


Figure 3: Proposed model for benchmark task. (a) and (b) show time-series data with  $u_k \in [-\sigma, \sigma]$  and  $[0, \sigma]$ , respectively. In (a) and (b), the solid black and solid red lines represent the output of the NARMA10 and the novel models, respectively. (c) and (d) show information processing capacity with  $u_k \in [-\sigma, \sigma]$  and  $[0, \sigma]$ , respectively. The labels represent combinations of  $[[n_i, k_i]]$ , where  $n_i$  is the degree of polynomial and  $k_i$  is the delayed time step of input. Here, the desired output is  $\prod_i \mathcal{P}_{n_i}(\nu_{k_i})$ .

model’s parameters. In addition, we introduced a model to resolve the problems associated with the NARMA10 model. The primary results are summarized as follows,

- Some settings for parameters  $(\alpha, \beta, \gamma, \delta, \mu, \sigma)$ , the initial values of  $\psi$ , and the input time-series  $u_k$  make the NARMA10 model converge to a saddle point; however, it can diverge probabilistically when the model output enters area (iv). When the output is in the vicinity of the fixed point, the Lyapunov exponent is negative and the model is predictable with input time-series  $\nu_k$ .
- The capacity distribution depends on some parameters. The capacity distribution with  $u_k \in [-\sigma, \sigma]$  only has capacities when the total degree of input  $\sum_i n_i = 2$ . In contrast, the distribution with  $u_k \in [0, \sigma]$  has capacities with  $\sum_i n_i = 1, 2$ , which vary depending on the magnitude of  $\sigma$ .
- As the NARMA10 model has the unstable region (iv), which does not depend on the parameters  $(\alpha, \beta, \gamma, \delta, \mu, \sigma)$ , and can diverge probabilistically to infinity, we have derived an approximate model represented by the low-degree Legendre polynomials. The approximate model is stable relative to the input range.

## References

- [1] Amir F Atiya and Alexander G Parlos. New results on recurrent network training: unifying the algorithms and accelerating convergence. *IEEE transactions on neural networks*, 11(3):697–709, 2000.



- [2] Lennert Appeltant, Miguel Cornelles Soriano, Guy Van der Sande, Jan Danckaert, Serge Massar, Joni Dambre, Benjamin Schrauwen, Claudio R Mirasso, and Ingo Fischer. Information processing using a single dynamical node as complex system. *Nature communications*, 2:468, 2011.
- [3] Filippo Maria Bianchi, Lorenzo Livi, Cesare Alippi, and Robert Jenssen. Multiplex visibility graphs to investigate recurrent neural network dynamics. *Scientific reports*, 7:44037, 2017.
- [4] Jens Bürger, Alireza Goudarzi, Darko Stefanovic, and Christof Teuscher. Hierarchical composition of memristive networks for real-time computing. In *Proceedings of the 2015 IEEE/ACM International Symposium on Nanoscale Architectures (NANOARCH'15)*, pages 33–38. IEEE, 2015.
- [5] François Duport, Anteo Smerieri, Akram Akrouf, Marc Haelterman, and Serge Massar. Fully analogue photonic reservoir computer. *Scientific reports*, 6:22381, 2016.
- [6] Keisuke Fujii and Kohei Nakajima. Harnessing disordered-ensemble quantum dynamics for machine learning. *Physical Review Applied*, 8(2):024030, 2017.
- [7] Michiel Hermans and Benjamin Schrauwen. Recurrent kernel machines: Computing with infinite echo state networks. *Neural Computation*, 24(1):104–133, 2012.
- [8] Michiel Hermans, Piotr Antonik, Marc Haelterman, and Serge Massar. Embodiment of learning in electro-optical signal processors. *Physical review letters*, 117(12):128301, 2016.
- [9] Masanobu Inubushi and Kazuyuki Yoshimura. Reservoir computing beyond memory-nonlinearity trade-off. *Scientific reports*, 7(1):10199, 2017.
- [10] Herbert Jaeger. Adaptive nonlinear system identification with echo state networks. In *Advances in neural information processing systems*, pages 609–616, 2003.
- [11] Kohei Nakajima, Helmut Hauser, Rongjie Kang, Emanuele Guglielmino, Darwin G Caldwell, and Rolf Pfeifer. Computing with a muscular-hydrostat system. In *2013 IEEE International Conference on Robotics and Automation*, pages 1504–1511. IEEE, 2013.
- [12] Kohei Nakajima, Helmut Hauser, Tao Li, and Rolf Pfeifer. Exploiting the dynamics of soft materials for machine learning. *Soft robotics*, 5(3):339–347, 2018.
- [13] Kohei Nakajima, Keisuke Fujii, Makoto Negoro, Kosuke Mitarai, and Masahiro Kitagawa. Boosting computational power through spatial multiplexing in quantum reservoir computing. *Physical Review Applied*, 11(3):034021, 2019.
- [14] Yvan Paquot, Francois Duport, Antoneo Smerieri, Joni Dambre, Benjamin Schrauwen, Marc Haelterman, and Serge Massar. Optoelectronic reservoir computing. *Scientific reports*, 2:287, 2012.
- [15] Ali Rodan and Peter Tino. Minimum complexity echo state network. *IEEE transactions on neural networks*, 22(1):131–144, 2010.
- [16] David Verstraeten, Benjamin Schrauwen, Michiel d’Haene, and Dirk Stroobandt. An experimental unification of reservoir computing methods. *Neural networks*, 20(3):391–403, 2007.
- [17] Jun Yin, Yan Meng, and Yaochu Jin. A developmental approach to structural self-organization in reservoir computing. *IEEE transactions on autonomous mental development*, 4(4):273–289, 2012.
- [18] Herbert Jaeger and Harald Haas. Harnessing nonlinearity: Predicting chaotic systems and saving energy in wireless communication. *science*, 304(5667):78–80, 2004.
- [19] Wolfgang Maass, Thomas Natschläger, and Henry Markram. Real-time computing without stable states: A new framework for neural computation based on perturbations. *Neural computation*, 14(11):2531–2560, 2002.
- [20] Matthew Dale, Julian F Miller, Susan Stepney, and Martin A Trefzer. Evolving carbon nanotube reservoir computers. In *International Conference on Unconventional Computation and Natural Computation*, pages 49–61. Springer, 2016.
- [21] Joni Dambre, David Verstraeten, Benjamin Schrauwen, and Serge Massar. Information processing capacity of dynamical systems. *Scientific reports*, 2:514, 2012.

## Supplementary material

### Approximate model

Here, we derive the following equations:

$$y_k = p + \sum_{i \in N_1} q_i \mathcal{P}_1(\nu_{k-i}) + \sum_{i \in N_2} r_i \mathcal{P}_1(\nu_{k-i}) \mathcal{P}_1(\nu_{k-i-9}) \quad (1)$$

$$p = \frac{1-\alpha}{20\beta} - \sqrt{\left(\frac{1-\alpha}{20\beta}\right)^2 - \frac{\gamma\mu^2 + \delta}{10\beta}} \quad (2)$$

$$q_i = \begin{cases} \sqrt{2/3} \gamma \mu \sigma (\alpha + 11\beta p)^i & (i = 0, \dots, 8) \\ \sqrt{2/3} \gamma \mu \sigma (1 + (\alpha + 11\beta p)^9) (\alpha + 11\beta p)^i & (i = 9, \dots) \end{cases} \quad (3)$$

$$r_i = \begin{cases} (2/3) \gamma \sigma^2 (\alpha + 11\beta p + \beta \gamma \mu^2)^i & (i = 0, 1) \\ (2/3) \gamma \sigma^2 (\alpha + 11\beta p + \beta \gamma \mu^2) (\alpha + 11\beta p)^{i-1} & (i = 2, \dots) \end{cases} \quad (4)$$

We expanded  $y_k$  using a normalized Legendre polynomial of input time-series  $\nu_{k-i}$ ,  $i = 1, \dots, k$  as follows:

$$y_k = p_k + \sum_{i=1}^k q_{k,i} \mathcal{P}_1(\nu_{k-i}) + \sum_{i=1}^k r_{k,i} \mathcal{P}_1(\nu_{k-i}) \mathcal{P}_1(\nu_{k-i-9}) + \dots, \quad (5)$$

where  $p_k$  denotes a term independent of  $\nu_{k-i}$ ,  $i = 1, \dots, k$  at the  $k$ -th time step, and  $q_{k,i}$  and  $r_{k,i}$  are the  $i$ -th coefficient of  $\mathcal{P}_1(\nu_{k-i})$  and  $\mathcal{P}_1(\nu_{k-i}) \mathcal{P}_1(\nu_{k-i-9})$  at the  $k$ -th time step, respectively. The NARMA10 model with  $\nu_k$  is represented by

$$y_{k+1} = \alpha y_k + \beta y_k \sum_{j=0}^9 y_{k-j} + \gamma (\mu + \sigma \nu_k) (\mu + \sigma \nu_{k-9}) + \delta. \quad (6)$$

According to Eqs. (5) and (6),  $y_{k+1}$  is rewritten to

$$\begin{aligned} y_{k+1} &= \alpha p_k + \beta p_k \sum_{j=0}^9 p_{k-j} + \gamma \mu^2 + \delta \\ &+ \sqrt{\frac{2}{3}} \gamma \mu \sigma \mathcal{P}_1(\nu_k) + \sqrt{\frac{2}{3}} \gamma \mu \sigma \mathcal{P}_1(\nu_{k-9}) + \sqrt{\frac{2}{3}} \sum_{i=1}^k \left( \alpha + \beta \left( p_k + \sum_{j=0}^9 p_{k-j} \right) \right) q_{k,i} \mathcal{P}_1(\nu_{k-i}) \\ &+ \frac{2}{3} \sigma^2 \mathcal{P}_1(\nu_k) \mathcal{P}_1(\nu_{k-9}) + \frac{2}{3} \beta q_{k,i} q_{k-9,i} \mathcal{P}_1(\nu_{k-1}) \mathcal{P}_1(\nu_{k-10}) \\ &+ \frac{2}{3} \sum_{i=1}^k \left( \alpha + \beta \left( p_k + \sum_{j=0}^9 p_{k-j} \right) \right) r_{k,i} \mathcal{P}_1(\nu_{k-i}) \mathcal{P}_1(\nu_{k-i-9}) + \dots \end{aligned} \quad (7)$$

Here, we used  $\mathcal{P}_1(\nu) = \sqrt{3/2} \nu$ . When increasing  $k$  by one in Eq.(5), we obtain a following equation:

$$y_{k+1} = p_{k+1} + \sum_{i=1}^k q_{k+1,i} \mathcal{P}_1(\nu_{k+1-i}) + \sum_{i=1}^k r_{k+1,i} \mathcal{P}_1(\nu_{k+1-i}) \mathcal{P}_1(\nu_{k+1-i-9}) + \dots \quad (8)$$

Equating the corresponding coefficients in Eqs. (7) and (8) results in

$$p_{k+1} = \alpha p_k + \sum_{i=0}^9 \beta p_k p_{k-i} + \gamma \mu^2 + \delta, \quad (9)$$

$$q_{k+1,i} = \begin{cases} \sqrt{2/3} \gamma \mu \sigma & (i = 0) \\ \left( \alpha + \beta (p_k + \sum_{j=0}^9 p_{k-j}) \right) q_{k,i-1} & (i > 0, i \neq 9) \\ \sqrt{2/3} \gamma \mu \sigma + \left( \alpha + \beta (p_k + \sum_{j=0}^9 p_{k-j}) \right) q_{k,i-1} & (i = 9) \end{cases}, \quad (10)$$

$$r_{k+1,i} = \begin{cases} (2/3) \gamma \sigma^2 & (i = 0) \\ \left( \alpha + \beta (p_k + \sum_{j=0}^9 p_{k-j}) \right) r_{k,i-1} + \beta q_{k,i} q_{k-9,i} & (i = 1) \\ \left( \alpha + \beta (p_k + \sum_{j=0}^9 p_{k-j}) \right) r_{k,i-1} & (i = 2, \dots) \end{cases}. \quad (11)$$

According to Eq. (9),  $p_k$  has a stable equilibrium point and an unstable one. If  $p_k < (1 - \alpha)/20\beta + \sqrt{((1 - \alpha)/20\beta)^2 - (\gamma \mu^2 + \delta)/10\beta}$ , it converges to the stable point. When  $k$  is large enough,  $p_k$  converges to

$$p = \lim_{k \rightarrow \infty} p_k = \frac{1 - \alpha}{20\beta} - \sqrt{\left( \frac{1 - \alpha}{20\beta} \right)^2 - \frac{\gamma \mu^2 + \delta}{10\beta}}. \quad (12)$$

According to Eq. (13),  $q_{k,i}$  also converges to

$$q_i = \lim_{k \rightarrow \infty} q_{k+1,i} = \begin{cases} \sqrt{2/3} \gamma \mu \sigma & (i = 0) \\ (\alpha + 11\beta p) q_{i-1} & (i > 0, i \neq 9) \\ \sqrt{2/3} \gamma \mu \sigma + (\alpha + 11\beta p) q_{i-1} & (i = 9) \end{cases}. \quad (13)$$

Therefore, we obtain

$$q_i = \begin{cases} \sqrt{2/3} \gamma \mu \sigma (\alpha + 11\beta p)^i & (i = 0, \dots, 8) \\ \sqrt{2/3} \gamma \mu \sigma (1 + (\alpha + 11\beta p)^9) (\alpha + 11\beta p)^i & (i = 9, \dots) \end{cases}. \quad (14)$$

In the same manner,  $r_{k,i}$  converges to

$$r_i = \lim_{k \rightarrow \infty} r_{k+1,i} = \begin{cases} (2/3) \gamma \sigma^2 & (i = 0) \\ (\alpha + 11\beta p) r_{i-1} + \beta q_{i-1}^2 & (i = 1) \\ (\alpha + 11\beta p) r_{i-1} & (i = 2, \dots) \end{cases} \quad (15)$$

$$= \begin{cases} (2/3) \gamma \sigma^2 (\alpha + 11\beta p + \beta \gamma \mu^2)^i & (i = 0, 1) \\ (2/3) \gamma \sigma^2 (\alpha + 11\beta p + \beta \gamma \mu^2) (\alpha + 11\beta p)^{i-1} & (i = 2, \dots) \end{cases}. \quad (16)$$

Therefore, when  $k$  is large enough and we approximate Eq. (5) with the constant term and the terms of  $\mathcal{P}_1(\nu_{k-i})$  and  $\mathcal{P}_1(\nu_{k-i})\mathcal{P}_1(\nu_{k-i-9})$  whose delayed time steps  $i$  are limited to sets  $N_1$  and  $N_2$ , respectively, we obtain Eqs. (1)-(4).

### Stability diagrams

Here, the discrete derivatives  $\Delta w_{1,k}$  and  $\Delta w_{2,k}$  are given again as follows:

$$\Delta w_{1,k} = (\alpha - 1)w_{1,k} + \beta w_{1,k} w_{2,k} + \delta, \quad (17)$$

$$\Delta w_{2,k} = \alpha w_{1,k} + \beta w_{1,k} w_{2,k} + \delta - z_{10,k}. \quad (18)$$

From these equations, nullclines are obtained as follows:

$$w_{2,k} = \frac{1 - \alpha}{\beta} - \frac{\delta}{\beta w_{1,k}}. \quad (19)$$

$$w_{2,k} = -\frac{\alpha}{\beta} + \frac{z_{10,k} - \delta}{\beta w_{1,k}}, \quad (20)$$

The intersection point of the nullclines is  $(w_1, w_2) = (z_{10}, (1 - \alpha)/\beta - \delta/\beta z_{10})$ . As  $z_{10,k}$  depends on time step  $k$ , the nullcline in Eq. (20) changes over time and has three outlines: i)  $z_{10,k} < \delta$ , ii)  $z_{10,k} = \delta$ , and iii)  $z_{10,k} > \delta$  (Figure S1). The signs of  $\Delta w_1$  and  $\Delta w_2$  are shown in Table S1-S3.

Table S1: Derivative table of  $\Delta w_1$  and  $\Delta w_2$  in stability diagram ( $z_{10} > \delta$ ; Figure S1(a))

# area	$\Delta w_1$	$\Delta w_2$	# area	$\Delta w_1$	$\Delta w_2$	# area	$\Delta w_1$	$\Delta w_2$
(i)	-	-	(iii)	+	+	(v)	-	+
(ii)	+	-	(iv)	+	+	(vi)	-	-

Table S2: Derivative table of  $\Delta w_1$  and  $\Delta w_2$  in stability diagram ( $z_{10} = \delta$ ; Figure S1(b))

# area	$\Delta w_1$	$\Delta w_2$	# area	$\Delta w_1$	$\Delta w_2$	# area	$\Delta w_1$	$\Delta w_2$
(i)	-	-	(iv)	+	+	(vii)	-	+
(ii)	+	-	(v)	-	+			
(iii)	+	+	(vi)	+	-			

Table S3: Derivative table of  $\Delta w_1$  and  $\Delta w_2$  in stability diagram ( $z_{10} < \delta$ ; Figure S1(c))

# area	$\Delta w_1$	$\Delta w_2$	# area	$\Delta w_1$	$\Delta w_2$	# area	$\Delta w_1$	$\Delta w_2$
(i)	-	-	(iii)	-	+	(v)	-	+
(ii)	+	-	(iv)	+	+	(vi)	-	-

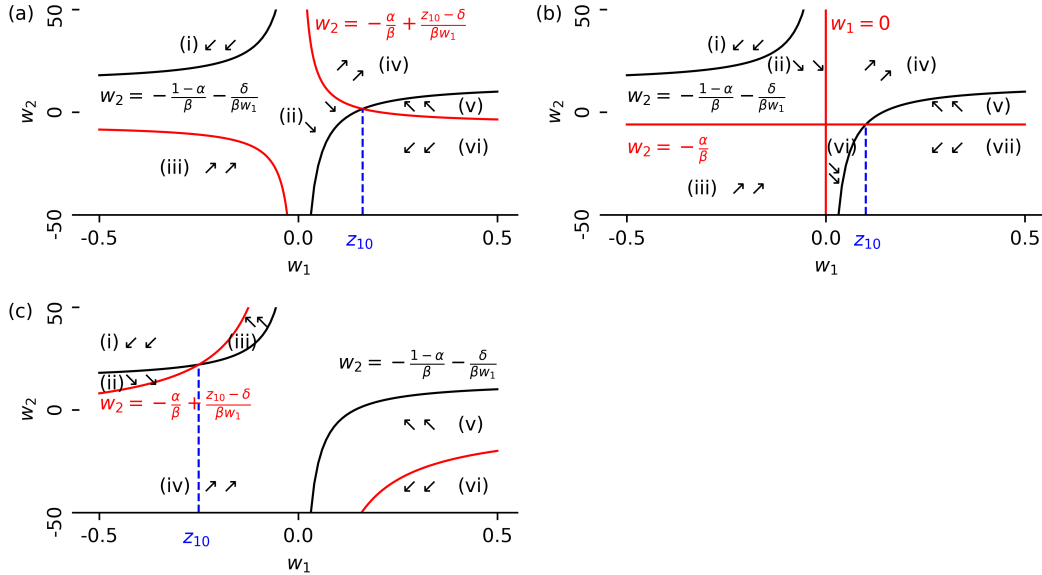


Figure S1: Stability diagram. The solid black and solid red lines represent  $\Delta w_1 = 0$  and  $\Delta w_2 = 0$ , respectively. The signs of  $\Delta w_1$  and  $\Delta w_2$  in (a), (b), and (c), are shown in Table S1, S2, and S3, respectively. In (a), (b), and (c), stability diagram of  $w_1$  and  $w_2$  as  $z_{10} < \delta$ ,  $z_{10} = \delta$ , and  $z_{10} > \delta$ , respectively. Note that the intersection point of nullclines is  $(w_1, w_2) = (z_{10}, (1 - \alpha)/\beta - \delta/\beta z_{10})$ .